frontiers | Frontiers in Chemical Biology

TYPE Original Research
PUBLISHED 28 February 2024
DOI 10.3389/fchbi.2024.1338630

OPEN ACCESS

EDITED BY
Richard C. Holz,
Colorado School of Mines, United States

REVIEWED BY
Urszula Katarzyna Komarnicka,
University of Wrocław, Poland
Luis A. E. Batista de Carvalho,
University of Coimbra, Portugal

*CORRESPONDENCE
C. N. Banti,
cbanti@uoi.gr
S. K. Hadjikakou,
shadjika@uoi.gr

RECEIVED 14 November 2023
ACCEPTED 02 February 2024
PUBLISHED 28 February 2024

CITATION
Banti CN, Tasiopoulos AJ and Hadjikakou SK (2024), Conjugation of an anti-metabolite nucleobase analogue with a mitochondriotropic agent via palladium(II) against breast cancer cells.
Front. Chem. Biol 3:1338630.
doi: 10.3389/fchbi.2024.1338630

Conjugation of an anti-metabolite nucleobase analogue with a mitochondriotropic agent via palladium(II) against breast cancer cells

C. N. Banti[1]*, A. J. Tasiopoulos[2] and S. K. Hadjikakou[1,3]*

[1]Inorganic and Analytical Chemistry, Department of Chemistry, University of Ioannina, Ioannina, Greece, [2]Department of Chemistry, University of Cyprus, Nicosia, Cyprus, [3]Institute of Materials Science and Computing, University Research Center of Ioannina (URCI), Ioannina, Greece

The conjugation of the uracil (a nucleobase) analogue, 6-methyl-thiouracil (MTUC), with the mitochondriotropic agent of Tri-o-Tolyl-Phosphine (TOTP) through palladium(II) leads to the formation of the metallodrug of formula [PdCl(TOTP)(MTUC)] (**1**). The metallodrug was characterized in solid state using Attenuated Total Reflectance-Fourier Transform Infra-Red (ATR-FTIR) spectroscopy and X-ray diffraction crystallography (XRD), while its behavior in solution was examined through Ultra Violet (UV) and ^{1}H NMR spectroscopies. The *in vitro* cytotoxicity of **1** was assessed against human breast adenocarcinoma cell lines: MCF-7 (hormone-dependent (HD)) and MDA-MB-231 (hormone-independent (HI)), as well as fetal lung fibroblast (MRC-5) cells. The MCF-7 cell morphology suggests apoptotic pathway, and this was confirmed by Acridine Orange/Ethidium Bromide (AO/EB) Staining, and the loss of the permeabilization of the mitochondrial membrane. The binding affinity of 1 toward the calf thymus (CT) DNA was clarified.

KEYWORDS

bioinorganic chemistry, palladium(II), mitochondriotropic agent, antiproliferative activity, apoptosis

1 Introduction

There's undeniable interest in platinum-based metallodrugs because of their proven and enduring use in clinical settings for treating various types of cancers. While platinum(II) metallodrugs make up 50% of all antineoplastic drugs, their utilization is restricted because of associated side effects such as severe nephrotoxicity, hepatotoxicity, neurotoxicity, and ototoxicity (Alam and Huq, 2016; Bomfim et al., 2019). While platinum(II) metallodrugs make up 50% of all antineoplastic drugs, their utilization is restricted because of associated side effects such as severe nephrotoxicity, hepatotoxicity, neurotoxicity, and ototoxicity (Garoufis et al., 2009; Fanelli et al., 2016). Given the resemblance in coordination modes and chemical properties between Pt(II) and Pd(II), a parallel biological behavior is anticipated (Garoufis et al., 2009; Fanelli et al., 2016). Typically, palladium forms complexes that share a geometric similarity with platinum complexes, albeit with different kinetics and stability, often at a lower cost (Garoufis et al., 2009; Fanelli et al., 2016). Compounds containing Pd(II) with diverse ligands featuring various donor atoms have demonstrated a range of activities including antitumor, anti-inflammatory, antibacterial, antiviral, and antifungal

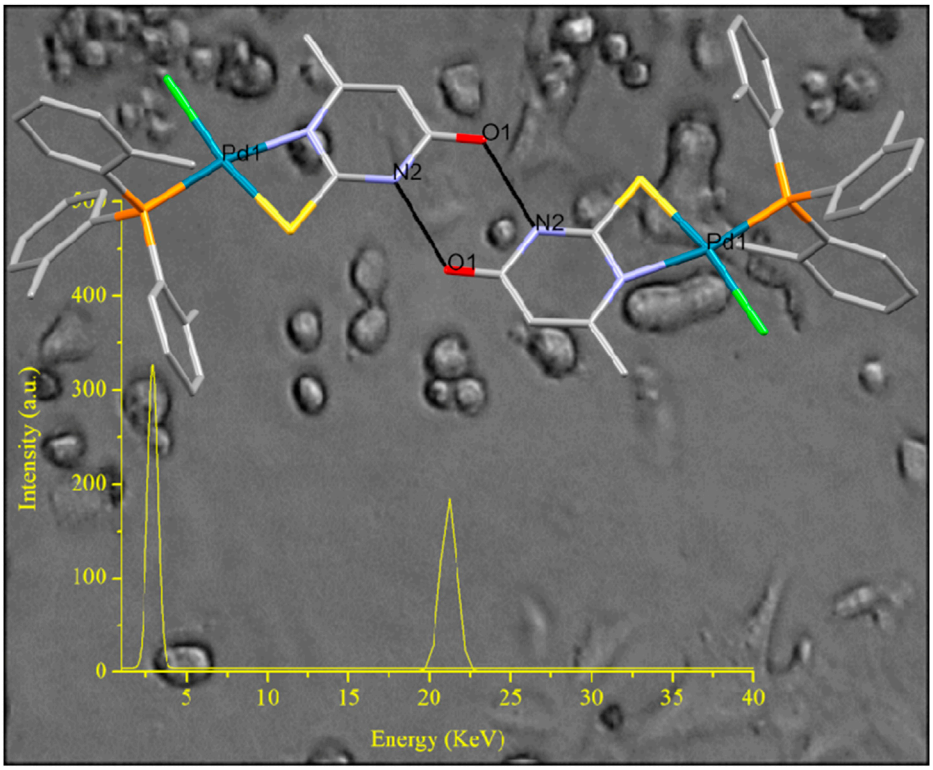

GRAPHICAL ABSTRACT
The conjugation of an anti-metabolite, nucleobase analogue, with a mitochondriotropic agent, via palladium(II) linker leads into a new less toxic, efficient targeted metallodrug for breast cancer antiproliferation which acts though apoptosis via mitochondrial-mediated pathway.

effects (Garoufis et al., 2009; Kapdi and Fairlamb, 2014; Banti et al., 2015; Fanelli et al., 2016; Lazarevic et al., 2017; Carneiro et al., 2020). In particular, numerous palladium or platinum complexes showcase cytotoxicity against tumor cells resistant to cisplatin, sometimes exhibiting superior activity compared to cisplatin itself (Garoufis et al., 2009; Hernández et al., 2016; Pruchnik et al., 2016; Espino et al., 2020; Schlagintweit et al., 2021; Bera et al., 2022; Priyanka Dorairaj et al., 2022; Chen et al., 2023; Haribabu et al., 2023; Wang et al., 2023).

The discovery and development of new therapeutic agents have recently ventured into a significant new realm by aiming to amalgamate two distinct classes of chemical agents into a unified entity through a linker (Blanco and Gardinier, 2020; Blanco, 2023). This combination of disparate agents offers the potential for synergistic effects. One of the prominent domains fostering innovative synergistic therapeutic modalities is the Conjugation of Metals with specific classes of Drugs (CoMeD) (Banti et al., 2016; Banti et al., 2023). Over the past two decades, mitochondria have emerged as a primary pharmacological target in the development of new cancer chemotherapeutics. They trigger cell apoptosis via the intrinsic pathway (Zielonka et al., 2017; Zhu et al., 2019). The accumulation of positively charged compounds within the mitochondrial matrix is facilitated by the negative inner membrane potential (Zhu et al., 2019). Mitochondriotropic lipophilic cations, like trialkyl derivatives of pnictogens (Ar_3E, where E= P, As, Sb), are specifically targeted to mitochondria, resulting in the disruption of mitochondrial membrane permeability (Banti et al., 2016; Banti et al., 2023). Furthermore, the anti-metabolite, exemplified by the nucleobase analogue 2-thiouracil (TUC) and its derivatives are utilized in crafting and advancing targeted anticancer metallodrugs. This is attributed to its ability to recognize nuclear DNA, consequently engaging in nucleobase anabolism (Correa et al., 2019). Hence, there's considerable interest in the biological assessment of metallodrugs resulting from the conjugation of mitochondriotropic pnictogen derivatives (like phosphorus) with a nucleobase analogue (such as derivatives of 2-thiouracil). Additionally, only three instances of conjugates between triarylphosphine and 2-thiouracil derivatives through Pd(II) have been documented in the CCDC, where the investigation into antiproliferative activity has been conducted so far (Groom et al., 2016).

During our research endeavors aimed at creating novel metal-based therapeutics for chemotherapy through the Conjugation of Metals with Drugs (CoMeD) (Banti et al., 2015; Banti et al., 2016; Chrysouli et al., 2018; Stathopoulou et al., 2021; Kapetana et al., 2022; Banti et al., 2023), the palladium(II) metallodrug of the formula [PdCl(TOTP)(MTUC)] (TOTP= Tri-o-Tolyl-Phosphine and MTUC= 6-methyl-thiouracil (Scheme 1)) was synthesized and characterized. The synergy, by the conjugate of the mitochondriotropic agent TOTP and the uracil analogue MTU, via Pd(II) ions, might lead to a better chemotherapeutic. The metallodrug was tested for its antiproliferative activity against human breast adenocarcinoma cell lines: MCF-7 (hormone dependent (HD)) and MDA-MB-231 (hormone independent (HI). The mechanism action was also elucidated.

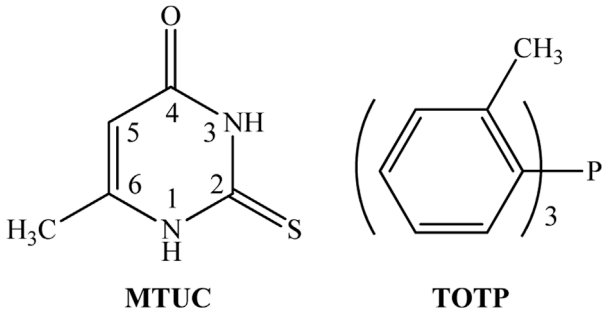

SCHEME 1
Ligands used.

2 Results and discussion

General Aspects: The compound is obtained by refluxing methanol/acetonitrile solution of palladium(II) dichloride, TOTP, and MTUC in a 1:1:1 ratio (Scheme 2). Orange crystals were collected from the mother solution. The formula of **1** was initially identified using spectroscopic methods, followed by refining its crystal structure through single-crystal X-ray diffraction analysis. These crystals remain stable when stored in darkness at room temperature. Additionally, the compound demonstrates solubility in methanol, acetonitrile, and DMSO.

2.1 Solid-state studies

Crystal and molecular structure of [PdCl(TOTP)(MTUC)] (**1**): ORTEP diagram of **1** along with selected bond distances and angles are shown in Figure 1.

The geometry around the Pd(II) is square planar. The MTUC chelates the metal center through its N,S-donor atoms forming a high-energy, four-membered ring. The distribution of bond lengths in **1** indicates the bond types depicted in Scheme 2. Specifically, the measured distance of the C23-O1 bond of 1.241 Å is notably closer to the reported length of 1.23 Å for a C=O double bond, as opposed to the C-O single bond length of 1.43 Å. The measured bond distances of C23-N2 at 1.402 Å, and C23-C24 at 1.414 Å indicate single rather than double bonds (typical lengths for single C-N and C-C bonds are 1.37 Å and 1.53 Å, respectively) (Scheme 2). The bond lengths C22-N2 at 1.350 Å, and N1-C25 at 1.369 Å tend towards the single C-N bond, while the C22-N1 at 1.316 Å is close to double C=N bond (typical lengths for double C=N is 1.27 Å). The C25-C24 bond length at 1.351 Å implies a double C=C bond (as depicted in Scheme 2). The measured C22-S1 bond length of 1.725 Å falls in the range of the C-S single bond (the typical length for a single C-S bond is 1.76 Å). Based on the bond length distribution, it is deduced that mono-deprotonation occurs at the N-C-S thioamide group of the MTUC upon its coordination with the Pd(II) metal center, as depicted in Scheme 2.

One P atom from the TOPT ligand, one Cl atom, and the N,S ones from MTUC form a square planar arrangement around the Pd(II) ion. The bond angles P-Pd-X (X= Cl and S) are close to the ideal value of 90° (Cl1-Pd1-P1= 90.22(6) and S1-Pd1-P1= 97.54(6))°, while the S1-Pd1-N1 varied significantly from the ideal 90° of a square planar geometry (S1-Pd1-N1= 69.69(15)°). The bond angles Cl1-Pd1-S1 (168.72(7)°) and P1-Pd1-N1 (167.11(15)°) lie away from the ideal value of 180°.

The Pd1-P1 bond length (2.2416(14) Å) is close to the corresponding distance found in previously reported compound with TPP of formula [$PdCl_2$(TPP)(MTUC)] (2.2363(8) Å) (Banti et al., 2015) and [$PdCl_2$(TPP)(TU)] (TU= thiourea) 2.2440(1) Å (Moro et al., 2006). The Pd1-S1 bond in **1**, is 2.3188(17) Å and is similar with the corresponding found in [$PdCl_2$(TPP)(MTUC)] (2.3197(9) Å)) and [$PdCl_2$(TPP)(TU)] (2.319(1) Å) (Moro et al., 2006). The length of the Pd-Cl bond (2.3170(16) Å) is in accordance with the corresponding ones, observed in [$PdCl_2$(TPP)(TU)] (Pd–Cl(l) 2.311(l), Pd–Cl(2) 2.401(l) Å) (Moro et al., 2006). Moreover, the Pd-Cl bond distance of **1** is close to the corresponding one in [$PdCl_2$(TPP)(MTUC)] ((Pd1–Cl1 = 2.3892(9), Pd1-Cl2 = 2.2892(9) Å) (Banti et al., 2015).

A robust intermolecular hydrogen bond O1···H[N2] at a distance of 2.752(7) Å connects two monomeric units of [PdCl(TOTP)(MTUC)], resulting in the formation of a dimer (depicted in Figure 1B). These robust hydrogen bonds could potentially facilitate a strong interaction between DNA and compound **1**.

Vibrational spectroscopy: The vibrational band at 1,620 cm^{-1} in the ATR-FTIR spectrum of MTUC is assigned to the ν(C=O) bond

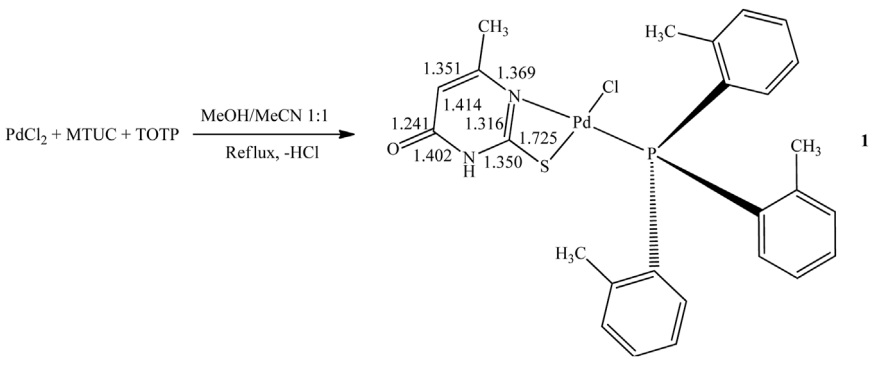

SCHEME 2
Synthesis of **1**.

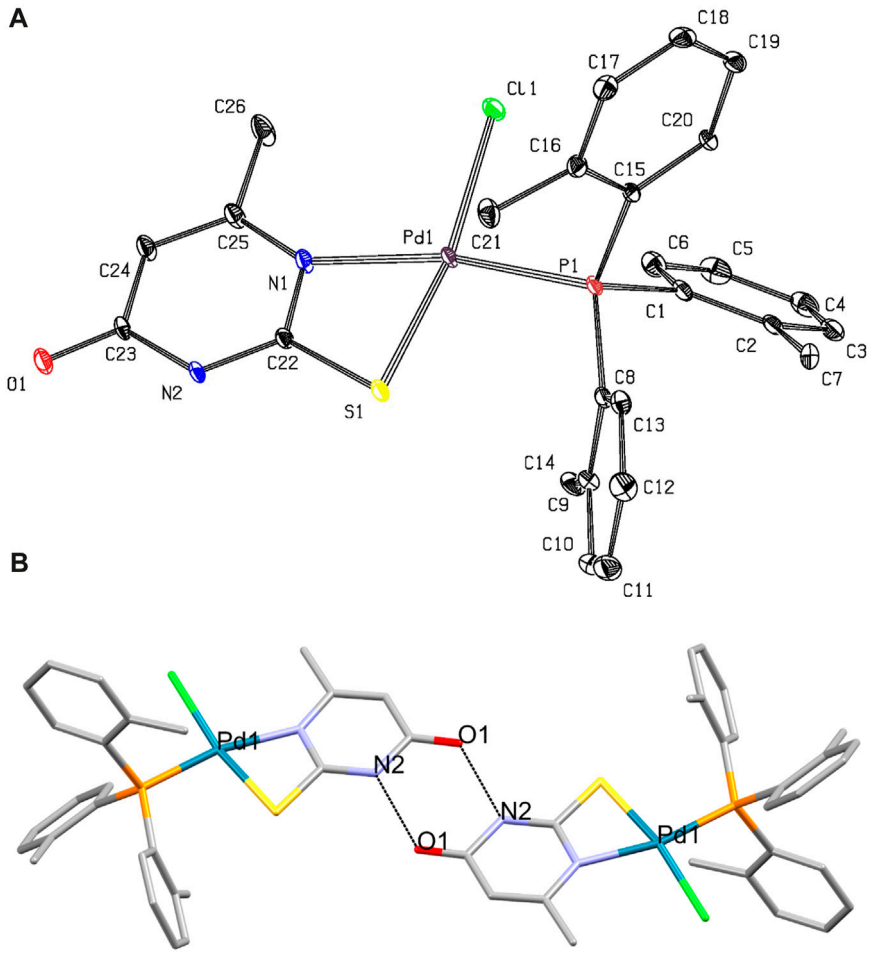

FIGURE 1
(A) ORTEP diagram of complex **1**. Selected bond lengths (Å) and angles (°): Pd1-Cl1= 2.3170(16), Pd1-S1= 2.3188(17), Pd1-P1= 2.2416(14), Pd1-N1= 2.148(5), Cl1-Pd1-S1= 168.72(7), Cl1-Pd1-P1= 90.22(6), Cl1-Pd1-N1= 102.67(15), S1-Pd1-P1= 97.54(6), S1-Pd1-N1= 69.69(15), P1-Pd1-N1= 167.11(15) **(B)** Dimer formed by strong intermolecular hydrogen bonds O1···H[N2]= 2.752(7) Å.

vibration which is shifted at 1,651 cm^{-1} in the spectrum of **1**. This validates the increase in the C=O bond order as shown by the bond distribution outlined in Scheme 2. The bands at 1,552 and 1,240 cm^{-1} in the ATR-FTIR spectrum of MTUC are assigned to the thioamide I (δ(N–H) + ν(C-N)) and II (ν(C–N) + δ(N–H) + ν(C=S)) bands (Aulakh et al., 2019), which mainly consisted as ν(ring), bond vibrations (Grosmaire and Delarbre, 2012). The bands at 990 and 654 cm^{-1} in the IR spectrum of MTUC are attributed to the ν(ring), ν(CS) vibrations (thioamide III (ν(C–N) + ν(C–S)) and IV (ν(C–S) bands) (Supplementary Figure S1) (Grosmaire and Delarbre, 2012; Charalampou et al., 2014; Banti et al., 2015). These vibration bands are shifted at 1,517, 1,238, 1,000, and 662 cm^{-1}, respectively. The significant shift of the thioamide I vibrational band from 1,552 to 1,517 cm^{-1} is likely due to the elongation of the C=N upon coordination of MTUC to Pd(II) (Supplementary Figure S1). Both C=N and N-H contribute to the thioamide I band mentioned earlier. This stands as the most compelling evidence of MTUC coordination to the Pd(II) apparent in the FTIR spectrum, as the other shifts observed are comparatively minor. The upward shift of the thioamide band III to 1,000 cm^{-1} from 990 cm^{-1} is likely due to the elongation of the C-S bond resulting from the coordination of MTUC toward Pd(II). The bands at 555-514 cm^{-1} in the spectrum of free TOTP are attributed to the ν(C–P) vibrations which are shifted at 563-536 cm^{-1} (Supplementary Figure S1).

2.2 Solution studies

^{1}H Nuclear Magnetic Resonance (^{1}H NMR) Spectroscopy: The broad resonance signal in the ^{1}H-NMR spectrum of **1** at 12.85 ppm is attributed to the H(N^{1}) and H(N^{3}) protons of the MTUC. The corresponding signal is observed at 12.23 ppm in the free ligand (Scheme 1; Supplementary Figure S2). The single resonance signal at 5.65 ppm is attributed to the H(C^{5}) of MTUC and it is shifted at 5.72 ppm in **1**. The singlet signal at 2.03 ppm is assigned to the H(CH_3-) of the methyl-substituent of MTUC. This signal is shifted at 1.64 ppm in **1** (Charalampou et al., 2014; Banti et al., 2015). The resonance signals at 7.54–6.92 and 2.22 ppm in the spectra of **1** are attributed to Haromatic and H(CH_3) of TOPT, respectively. The corresponding signals of the free TOPT are observed at 7.28–6.55 and 2.27 ppm, respectively (Banti et al., 2016) (Supplementary Figure S2).

TABLE 1 IC_{50} values of complexes of palladium(II), silver(I) and copper(I) with thiouracil and triphenylphosphine.

Compound	IC_{50} value (μM)						Ref.
	MCF-7	MDA-MB 231	MRC-5	MG63	A549	HeLa	
1	39.1 ± 1.3	57.1 ± 3.4	38.1 ± 2.9				[a]
cis-Cl-[$PdCl_2$(TPP)(MTUC)]·3(H_2O)	>30	-				>30	Banti et al. (2015)
[PdCl(TPP)(*μ-N,S*-TUC)PdCl$(TPP)_2$]	21.0						Shaheen et al. (2007)
[PdCl(TPP)(*N,S*-TUC)]	4.6						Shaheen et al. (2007)
[Ag(TUC)$(TPP)_2$](NO_3)·H_2O)				16.6			Aulakh et al. (2019)
[CuCl$(TPP)_2$(eitotH_2)]			5.0		5.6	3.6	Papazoglou et al. (2014)
[CuBr$(TPP)_2$(eitotH_2)]			4.8		4.7	3.4	Papazoglou et al. (2014)
[CuI$(TPP)_2$(eitotH_2)]			6.8		5.0	2.6	Papazoglou et al. (2014)
cisplatin	5.50 ± 0.40	26.7 ± 1.1	1.1 ± 0.2			3.9 ± 0.1	Banti et al. (2016)

[a]In this work, TPP, triphenylphosphine; TUC, 2-thiouracil, eitotH_2= 5-carbethoxy-2-thiouracil.
The compounds lacking standard deviations in their IC_{50} values, are derived from independent literature sources, not our group's data. Hence, it is not possible for us to include standard deviations within these values. The IC_{50} values of cisplatin along with their corresponding standard deviations presented in the table are outcomes derived from our group's research. The conditions, materials, and methodology employed to ascertain these values align with those described in this paper.

Stability studies: The stability of **1** was verified by UV and ^{1}H-NMR spectroscopies for a period of 48 h (Supplementary Figures S3, S4), which corresponds to the period of incubation of the cells with the compound. No changes were observed between the initial spectra and the corresponding ones after 48 h, confirming the retention of its structure in solution.

2.3 Biological studies

In vitro antiproliferative activity: The *in vitro* antiproliferative activity of **1** was evaluated against two human adenocarcinoma breast cell lines, MCF-7 (hormone depended (HD)) and MDA-MB-231 (hormone independent (HI)) by sulforhodamine B (SRB) assay after its incubation for 48 h. The IC_{50} values of **1** against MCF-7 and MDA-MB 231 cells are 39.1 ± 1.3 and 57.1 ± 3.4 μM, respectively (Table 1). The corresponding IC_{50} value exhibited by cisplatin against MCF-7 and MDA-MB 231 cells is 5.5 ± 0.4 and 26.7 ± 1.1 μM, respectively, suggesting lower antiproliferative activity of **1**. The low activity of **1** follows the corresponding one of *cis-Cl*-[$PdCl_2$(TPP)(MTUC)]·3(H_2O), which shows no antiproliferative activity up to the concentration of 30 μM tested (Banti et al., 2015).

The heteroleptic palladium(II) complexes of 2-thiouracil and TPP, [PdCl(TPP)(*μ-N,S*-TUC)PdCl$(TPP)_2$] and [PdCl(TPP)(*N,S*-TUC)] (Shaheen et al., 2007) were assessed across a selection of seven human tumor cell lines: MCF-7 and EVSA-T (two breast cancers), WiDr (colon cancer), IGROV (ovarian cancer), M19 MEL (melanoma), A248 (renal cancer), and H226 (non-small cell lung cancer). Their IC_{50} values spanned a range from 0.4 to 25.1 μM. Particularly, the IC_{50} values of [PdCl(TPP)(*μ-N,S*-TUC)PdCl$(TPP)_2$] and [PdCl(TPP)(*N,S*-TUC)] against MCF-7 cells, are 21.0 and 4.6 μM (Shaheen et al., 2007) (Table 1). Moreover, the IC_{50} value of the silver(I) complex of 2-thiouracil (TUC) [Ag(TUC)$(TPP)_2$](NO_3)·H_2O) against human osteosarcoma cells (MG63) is 16.6 μM (Aulakh et al., 2019) (Table 1), while the corresponding one of copper(I) halide complexes with 5-carbethoxy-2-thiouracil (eitotH_2), [CuX(eitotH_2)$_2$]$_2$ and [CuX$(TPP)_2$(eitotH_2)] (X= Cl, Br, I) against A549 (human pulmonary carcinoma cell line), HeLa (human epithelial carcinoma cell line) and MRC5 cells range between 3.4 and 118 μM (Papazoglou et al., 2014) (Table 1). The copper compounds of TPP show higher antiproliferative activity than those without TPP. Generally, the palladium(II) compounds with MTUC or TUC exhibit antiproliferative activity in higher concentrations than those of silver or copper complexes.

The *in vitro* toxicity of **1** was also estimated against normal human fetal lung fibroblast cells (MRC-5). Its IC_{50} value is 38.1 ± 2.9 μM (Table 1). This led to a Therapeutic Potency Index (TPI= (IC_{50} agent against non-cancerous cells)/(IC_{50} against cancerous cells)) of 0.98, against MCF-7 (HD) and 0.50 against MDA-MB-231(HI), respectively. The TPI values of cisplatin against MCF-7 (HD) and MDA-MB-231(HI) are 0.20 and 0.04. Therefore, **1** exhibits higher selectivity for cancer cells than for normal ones, while it is less toxic, towards MRC-5 cells, than cisplatin by 35-fold.

In vitro Mechanism of Action. The *in vitro* mechanism of action for **1** is elucidated through (i) Pd(II) localization (ii) observation of MCF-7 cell morphology, (iii) staining with acridine orange/ethidium bromide (AO/EB), and (iv) conducting a mitochondrial membrane permeabilization test.

[i] *Pd(II) localization*: In an attempt to ascertain if the palladium metallodrug penetrates the cytoplasm, we conducted X-ray fluorescence spectroscopy (XRF) measurements. The XRF spectrum of **1** confirms the presence of Pd in the cytoplasm (Supplementary Figure S5). The outcomes indicated that, following incubation of MCF-7 cells with the metallodrug at a concentration of 4.13 ppm, the cytoplasm contained approximately 3.2 ± 0.4 ppm of palladium. Before quantifying the palladium, the cells underwent a triple wash with PBS to remove the medium, followed by centrifugation each time. At present we lack the tools, such as luminescence tracers or

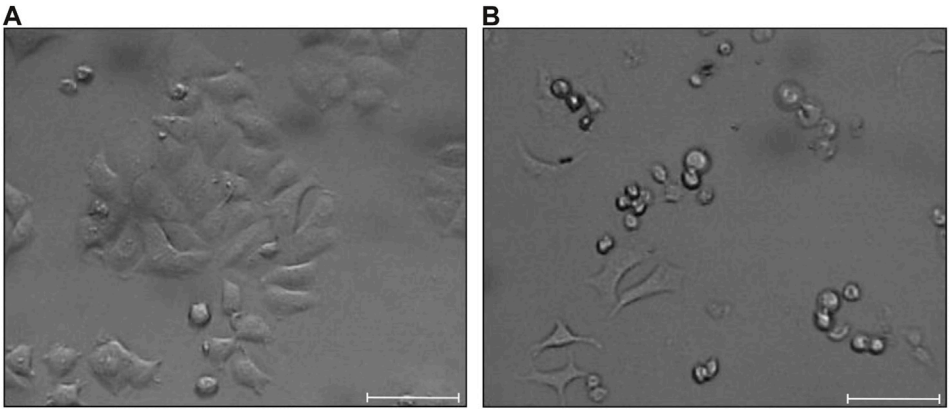

FIGURE 2
MCF-7 cells morphology **(A)** and their morphological alterations observed upon treatment with **1 (B)**. Scale bar is 100 μm.

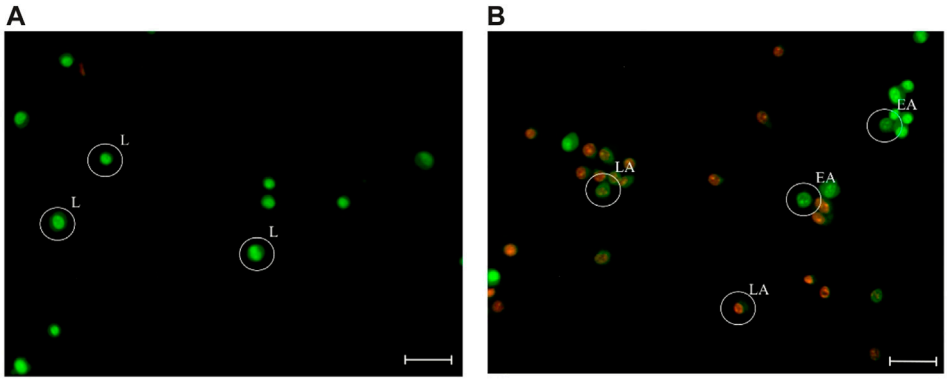

FIGURE 3
Fluorescence images of the untreated MCF-7 cells **(A)**, and those incubated with **1** at IC_{50} value, in 37°C for 48 h **(B)**, stained with AO/EB. "L" indicates live cells; "EA" indicates early apoptotic cells; "LA" indicates late apoptotic cells. Scale bar is 100 μm.

confocal microscopy, to precisely track the Pd compound's localization to demonstrate its selective targeting of DNA. Furthermore, the Pd(II) metallodrug, when excited at λ_{exc}= 367 nm, emits no radiation between 380 and 700 nm hindering its identification within DNA via its own fluorescence (Supplementary Figure S6).

[ii] *Cell morphology studies:* The morphological differences of the incubated MCF-7 cells upon **1** at its IC_{50} value, were detected under an inverted microscope (Figure 2). Differences in cell morphology were detected in treated in contrast to untreated MCF-7 cells. The untreated cells are elongated, adherent, and showed cellular crowding. The treated cells, on the other hand, show cell shrinkage, detachment, and rounding up, the cell contact is lost, and they form islets of more rounded cells (Banti et al., 2016; Chrysouli et al., 2018; Stathopoulou et al., 2021; Kapetana et al., 2022; Banti et al., 2023). The observational experiment displayed that the MCF-7 cells exposed to **1** showed more destructive changes in their morphology compared to untreated cells. Therefore, an apoptotic type of MCF-7 cell death is suspected after their treatment with **1.**

[iii] *AO/EB staining assay:* The investigation into the cell death mechanism triggered by **1** in MCF-7 cells was explored through the AO/EB staining assay (Figure 3). AO is a fluorescent dye that permeates cells and stains nuclear DNA in both living and deceased cells, whereas EB solely stains cells with compromised membrane integrity (Kasibhatla et al., 2006). In untreated cells, a consistent green fluorescence was visible within the nucleus. However, in instances of apoptosis, early apoptotic cells exhibited a greenish-yellow tint or displayed green-yellow fragments, while late apoptotic cells appeared orange or showed orange fragments.

Upon treatment of MCF-7 cells by **1**, a significant increase in apoptosis was observed. The percentage of apoptotic cells is (58.0 ± 7.9) % in contrast to the untreated cells (17.1 ± 1.0) %. No necrotic cells were observed (Afsar et al., 2016). Therefore, it is concluded that the antitumor activity of **1** was triggered due to apoptosis instead of the necrosis pathway.

[iv] *Loss of the mitochondrial membrane permeabilization (MPP):* To investigate whether the metallodrug **1** interferes with

mitochondrion, the loss of mitochondrial membrane permeabilization (MMP), which is an indicator of mitochondrial dysfunction, was measured. The fluorescence of the cationic mitochondriotropic dye, which bioaccumulates in the membrane of the normal mitochondrion, and quenchs when MMP collapses with a consequent release of cytochrome c in the cytosol activating the apoptotic pathway.

The % quenching of the fluorescence emitted when MCF-7 cells are treated with **1** is 18.7%. Upon treatment of the cells with [$PdCl_2$(TPP)(MTUC)] the fluorescence emitted quench by only 8.2%. The fluorescence quenching caused by cisplatin, rises up to 54.9% (Chrysouli et al., 2018). These observations provide additional validation for the previously inferred apoptosis detected through cell morphology and the acridine/ethidium assay. Certainly, the quenching in fluorescence emitted from the dye, which is bonded to the mitochondrial membrane, upon cell exposure to the Pd(II) metallodrug is not evidence of a direct interaction of the drug with the mitochondrial membrane. The loss in mitochondrial membrane permeabilization might arise from alternative pathways. However, it is crucial to demonstrate that the Pd(II) metallodrug either triggers these pathways or directly engages with them, ultimately leading to the loss of mitochondrial membrane permeabilization.

DNA Binding Studies: DNA has been extensively studied as a potential pharmacological target of metalotherapeutics. The DNA binding affinity towards **1** was investigated (Banti et al., 2015; Banti et al., 2016; Chrysouli et al., 2018; Stathopoulou et al., 2021; Kapetana et al., 2022; Banti et al., 2023). The DNA-**1** complex formation is studied here by (i) viscosity measurements, (ii) absorption titration, (iii) fluorescence spectroscopy and (iv) by the DNA Thermal Denaturation (Banti et al., 2015; Banti et al., 2016; Chrysouli et al., 2018; Stathopoulou et al., 2021; Kapetana et al., 2022; Banti et al., 2023).

Viscosity Studies: The preliminary understanding of the DNA interaction mode with **1** was initially derived from viscosity measurements. The viscosity of a DNA solution is highly responsive to alterations in DNA length, serving as a pivotal indicator of the DNA binding mode in solution, notably influenced by the formation of the DNA-1 complex (Kapetana et al., 2022; Banti et al., 2023). In the case of intercalation interaction, the DNA-agent solution experiences a notable rise in relative viscosity, attributable to the unwinding and elongation of the double helix (Kapetana et al., 2022; Banti et al., 2023). On the other hand, when groove binding or electrostatic interactions occur, there is an insignificant impact on DNA length, resulting in no significant change in viscosity (Kapetana et al., 2022; Banti et al., 2023). Moreover, when an agent induces DNA strand cleavage, the DNA length decreases, consequently leading to a significant decrease in viscosity (Kapetana et al., 2022; Banti et al., 2023). Lastly, if a covalent bond forms between an agent and DNA, such as in the case of cisplatin-DNA, the solution viscosity decreases due to kinking in the DNA backbone, shortening the axis length of the helix (Kapetana et al., 2022; Banti et al., 2023).

The values of relative specific viscosity $(n/no)^{1/3}$ were plotted vs. the values r= [complex]/[DNA] (Figure 4). The increasing amounts (up to r= 0.37) of **1** in the DNA solution increase its relative viscosity slightly. This indicates groove binding interaction. Intercalation mode of DNA interaction with a binder, on the other hand, would significantly

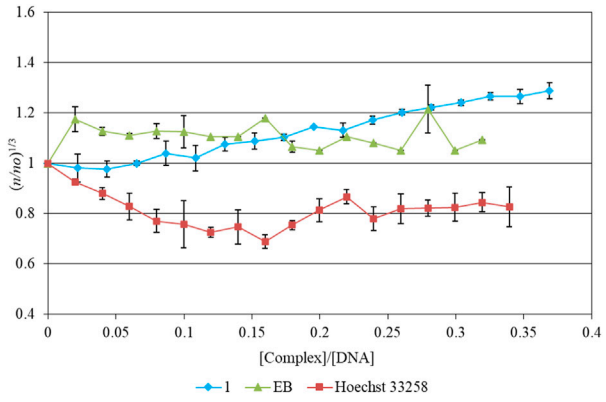

FIGURE 4
Relative viscosity of CT-DNA with increasing concentrations of **1**, Hoechst 33258 and Ethidium Bromide ([DNA]= 10 mM, r= [compound]/[DNA], n is the viscosity of DNA in the presence of the compounds and n_o is the viscosity of DNA alone).

increase the viscosity of the solution (Figure 4), e.g., in the case of the DNA-ethidium bromide (EB) interaction (Figure 4). The minor groove binding agent Hoechst 33258 leads to a moderate decrease of the DNA solution viscosity similar to the one observed in the case of DNA-**1** complex (Figure 4).

UV-Vis Spectroscopic study: Electronic absorption spectroscopy is used in the study of the binding properties (covalent, non-covalent, and electrostatic or groove binding mode) of metallodrugs with DNA.

The absorbance of CT-DNA (λ_{max}= 258 nm) was recorded upon the presence and absence of **1** at various r values (r = [agent]/[DNA]) at a constant [DNA] (Supplementary Figure S7). A slight hyperchromic effect was detected (3.4%), indicative of either slight groove binding or electrostatic mode (Banti et al., 2015; Banti et al., 2016; Chrysouli et al., 2018; Stathopoulou et al., 2021; Kapetana et al., 2022; Banti et al., 2023). The intrinsic binding constant (K_b) of **1** was calculated (1.1 ± 3.3)×10^4 M^{-1} (Supplementary Figure S8), while the corresponding metallodrug of TPP (cis-Cl-[$PdCl_2$(TPP)(MTUC)]·3(H_2O)) shows similar K_b value (4.5 ± 1.5)×10^4 M^{-1}, with slight also hyperchromicity effect at 258 nm (Banti et al., 2015). However, since the hydrolysis rate for palladium is faster than that of platinum complexes (10^5 times faster according to instrumental methods, and 10^6 times estimated by *ab initio* studies (Largy et al., 2011)), this leads to instability of Pd-DNA complexes relative to their Pt counterparts. This results in the limited use of Pd derivatives for DNA targeting and for biomedical applications (Largy et al., 2011). Generally, the absorption spectra indicated that the complex interacts with DNA weakly, and therefore a groove binding is concluded in accordance with the viscosity measurements (see above).

Fluorescence Spectroscopic Studies: The binding properties of **1** towards CT-DNA were further evaluated by fluorescence spectroscopic studies. Intercalative or minor groove binding mode can be detected by the quenching of fluorescence emitted from the CT-DNA/EB complex when the EB is substituted by a DNA binder (Banti et al., 2015; Banti et al., 2016; Chrysouli et al., 2018; Stathopoulou et al., 2021; Kapetana et al., 2022; Banti et al., 2023). The recorded emission spectra of the CT-DNA-EB complex upon excitation at λ_{exc} = 527 nm in the absence and presence of **1** are

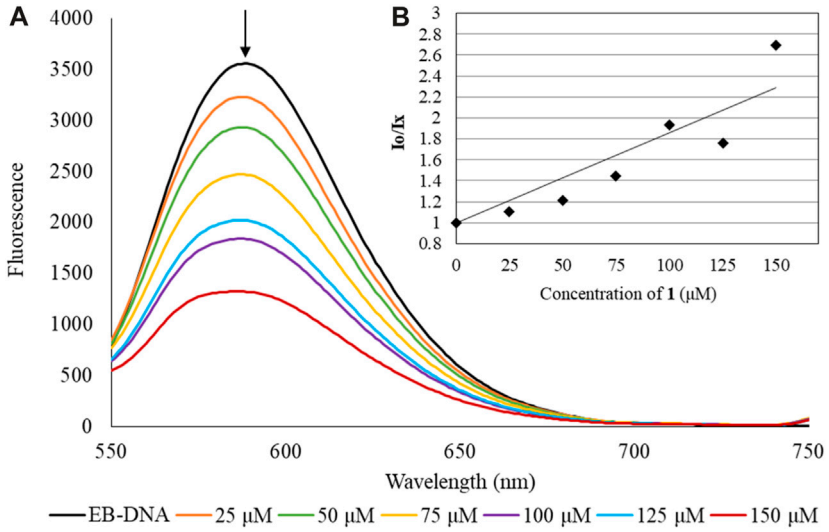

FIGURE 5
Emission spectrum **(A)** of CT-DNA-EB complex when undergoes excitation with λ_{exc}= 527 nm, in the presence of **1** ([EB]= 2.3 μM [DNA]= 26 μM [complex]= 0–150 μM)). The arrow shows the intensity changing upon increasing complex concentration. Inset **(B)** shows the plots of emission intensity I_0/I_x vs. [agent].

shown in Figure 5. The intensity of the radiation emitted at 588 nm forms the solution of the CT-DNA-EB complex undergoes quenching by 82%, by increasing the concentrations of **1**, as compared to the initial fluorescence intensity of the solutions EB-DNA. The Pd(II) metallodrug does not emit at λ_{em}= 588 nm when excited at λ_{exc}= 527 nm, having no impact on the corresponding emission of EB-DNA (Supplementary Figure S9). The value of the apparent binding constant (K_{app}) was calculated and the concentration of the drug at 50% reduction of the fluorescence is derived from the diagram of (I_x/I_0) (I_0 and I_x are the emission intensities of the CT-DNA-EB in the absence and presence of **1**, respectively) vs. the concentration of **1** (Figure 5) (Banti et al., 2015; Banti et al., 2016; Chrysouli et al., 2018; Stathopoulou et al., 2021; Kapetana et al., 2022; Banti et al., 2023). The K_{app} value is (29.8 ± 6.0)×10^4 M^{-1}) suggesting minor groove binding. The value of K_{app} lies in the range 10^4-10^5 M^{-1} implies groove binding mode (Sheng et al., 2007; Banti et al., 2015; Banti et al., 2016; Chrysouli et al., 2018; Stathopoulou et al., 2021; Kapetana et al., 2022; Banti et al., 2023). For comparison the corresponding K_{app} of EB is 10^7 M^{-1}, indicating that **1** binds through minor groove mode (Sheng et al., 2007; Banti et al., 2015; Banti et al., 2016; Chrysouli et al., 2018; Stathopoulou et al., 2021; Kapetana et al., 2022; Banti et al., 2023).

DNA Thermal Denaturation studies: Thermal denaturation studies of double-helical DNA to single-strands can be detected by a "hyperchromic effect" at 258 nm in the UV spectrum of the DNA with or without binder agents. A "sigmoid" melting transition curve is produced, simultaneously (Banti et al., 2024). As the temperature of DNA rises, the stacking interactions among bases and the hydrogen bonding between the bases in the double-stranded DNA gradually become disrupted (Banti et al., 2024). The DNA melting temperature (T_m) denotes the temperature at which half of the double-stranded DNA separates into two single strands, as the molar extinction coefficient of single-stranded DNA significantly exceeds that of double-stranded DNA (Banti et al., 2024).

The T_m of unbound DNA was found to be 59.5 ± 1.0°C (Figure 6). Under the same experimental conditions, the observed T_m of the DNA-**1** complex is 60.2 ± 0.5°C. The effect of **1** on the melting profile of CT-DNA was smaller than that produced by the well-known intercalator, ethidium bromide (EB), causing a considerable increase of T_m of DNA (ΔT_m of 13°C) (Cory et al., 1985; Kelly et al., 1985; Banti et al., 2024)). In the case of a groove binding or electrostatic interaction mode, the ΔT_m value is <2°C (Cory et al., 1985; Kelly et al., 1985; Banti et al., 2024). Since the ΔT_m value of the DNA-**1** complex is lower than 2°C, then a groove or electrostatic interaction mode can be concluded.

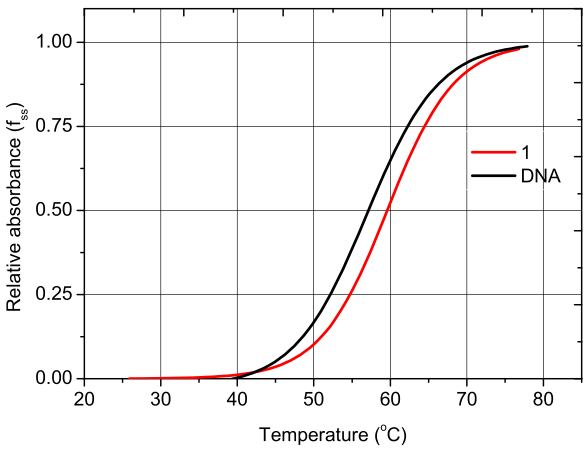

FIGURE 6
Melting curves of CT-DNA in the absence and presence of **1**, CT-DNA= 2.0 × 10^{-5} M; C_{drug} = 10^{-6} M in 1 mM trisodium citrate, 10 mM NaCl (pH= 7.0). Diagram of relative absorbance (f_{ss}) vs. temperature ((f_{ss} = (A-A_{min})/(A_{max}- A_{min}), where A_{min} is the minimal absorbance of the solution of CT-DNA-drug, at a temperature T, A is the absorbance of CT-DNA-drug corresponding to a specific temperature and A_{max} is the maximum absorbance of CT-DNA-drug, respectively).

3 Conclusion

The anti-metabolite of uracil analogue, 6-methyl-thiouracil, was conjugated with the mitochondriotropic agent of tri-o-tolyl-phosphine in one entity through palladium(II) ions towards the development of new metallodrug. X-ray crystallography reveals a square planar arrangement of the Cl-, μ-N,S-, P- donor atoms around the Pd(II) ion.

The compound was evaluated towards two types of breast cancer cells (hormone depended and independent). The compound exhibits 1.5-fold higher activity towards the hormone depended cell line (MCF-7) than against hormone independent one (MDA-MB 231). Given that both cell lines originated from the breast tissue, the antiproliferative activity of **1** might be involved in hormone receptors. The compound exhibits lower antiproliferative activity than cisplatin towards both cancerous cell lines. However, it exhibits higher selectivity for cancerous cells than for normal ones. Metallotherapeutic **1** is 35-fold less toxic than cisplatin against MRC-5 cells. Moreover, the palladium(II) compounds with MTUC or TUC such as **1**, *cis-Cl*-[$PdCl_2$(TPP)(MTUC)]·3(H_2O) or [PdCl(TPP)(μ-*N,S*-TUC)$PdCl(TPP)_2$] and [PdCl(TPP)(*N,S*-TUC)] (Shaheen et al., 2007; Banti et al., 2015) exhibit lower antiproliferative activity than that of silver or copper complexes. This might be due to the hydrolysis rate that palladium complexes undergo which is much faster in this case (Largy et al., 2011).

Along with compound **1**, only four occurrences of conjugates between triarylphosphine and 2-thiouracil derivatives via Pd(II) have been recorded in the CCDC (Groom et al., 2016), investigated for their antiproliferative activity (as detailed in Table 1) (Shaheen et al., 2007; Banti et al., 2015). Table 1 presents a summary of the antiproliferative activity of these conjugates involving triphenylphosphine with thiouracil derivatives via Pd(II), Ag(I), and Cu(I) in comparison to cisplatin (Shaheen et al., 2007; Papazoglou et al., 2014; Banti et al., 2015; Aulakh et al., 2019). The findings indicate lower potency of the Pd(II) compounds, particularly compound **1**. However, compound **1** exhibits significantly lower toxicity, being 7.6, 8.0, 5.6, and 35 times lower than that of [$CuCl(TPP)_2$(eitotH_2)], [$CuBr(TPP)_2$(eitotH_2)], [$CuI(TPP)_2$(eitotH_2)], and cisplatin, respectively (Table 1) (Shaheen et al., 2007; Papazoglou et al., 2014; Banti et al., 2015; Aulakh et al., 2019).

The Pd(II) compound induces apoptosis at a rate of (58.0 ± 7.9)%, a substantial increase compared to the untreated MCF-7 cells (17.1 ± 1.0)%, indicating alterations in cell morphology consistent with apoptosis. The loss of mitochondrial membrane permeability resulting from its direct or indirect interaction with **1** might imply apoptosis activation via the mitochondrial pathway. Moreover, the lower activity of these compounds might be assigned to the moderate interaction of **1** with DNA, through minor groove binding or electrostatic modes.

Hence, combining an anti-metabolite, nucleobase analogue, with a mitochondria-targeting agent using a palladium(II) linker results in a novel, metallodrug for inhibiting breast cancer proliferation via apoptosis, offering reduced toxicity.

4 Experimental

4.1 Materials and methods

Materials and Instruments: Reagent-grade solvents, such as 6-methyl-2-thiouacil (Aldrich) and tris(o-tolyl)phosphine (Sigma–Aldrich, Merck), were employed without additional purification. These included dimethyl sulfoxide, methanol, and acetonitrile from Riedel-de Haën, toluene from Sigma Aldrich-Merck, and dichloromethane from Panreac. Calf thymus (CT)-DNA and ethidium bromide (EB) were procured from Sigma-Aldrich. The MCF-7, MDA-MB-231, and MRC-5 cell lines used in this study were obtained from ATCC (American Type Culture Collection).

Melting point measurements were performed in open tubes using a Stuart Scientific apparatus and remain uncorrected. Elemental analyses for carbon and hydrogen were conducted using the Carlo Erba EA MODEL 1108 elemental analyzer. The Cary 630 ATR-FTIR spectrometer by Agilent Technologies was employed to record infrared spectra ranging from 4,000 to 400 cm^{-1}. The spectrometer's resolution, ranging from 2–16 kaiser, was set at 4 cm^{-1} for the experiments. This specific instrument configuration features a KBr beam splitter, incorporates a diamond crystal, and utilizes a DTGS (Deuterated Triglycine Sulfate) detector. The ^{1}H NMR spectra were acquired using a Bruker AC 250 MHz FT-NMR instrument in DMSO-d_6 solution, with chemical shifts (δ) reported in parts per million (ppm) using $(CH_3)_4Si$ as an internal reference. Electronic absorption spectra were recorded at 450 to 190 nm in DMSO and Buffer solution using a VWR UV-1600 PC series spectrophotometer. Fluorescence spectra were captured at 700 to 380 nm in DMSO and Buffer solution irradiating with λ_{ex}= 367 or 527 nm utilizing a Jasco FP-8200 Fluorescence Spectrometer. XRF measurements were carried out employing a Rigaku NEX QC EDXRF analyzer situated in Austin, TX, USA using $PdCl_2$ for the standard curve.

Synthesis and crystallization of **1**: For the preparation of complex **1**, 0.50 mmol of $PdCl_2$ (0.09 g), 0.50 mmol of tris(o-tolyl)phosphine (0.152 g) and 0.50 mmol of 6-methyl-2-thiouacil (MTUC) (0.07 g) were suspended to 20 cm^3 methanol/acetonitrile solution (1:1) under continues stirring and reflux for 3 h. The solution was then filtered off and the filtrate was kept in ambient condition. Crystals suitable for X-ray analysis were grown from the mother solution after a few days.

1: Orange crystals; Elemental analysis found: C: 53.75; H: 4.33; N: 4.57, P: 5.49; Pd: 18.23; S:5.18%; calculated for $C_{26}H_{26}ClN_2OPPdS$: C: 53.71; H: 4.46; N: 4.77, P: 5.27; Pd: 18.11; S:5.46%; IR (cm^{-1}): 1649vs, 1518m, 1449m, 1399m, 1363s, 1280m, 1239s, 1192s, 1131m, 1044m, 1001m, 956m, 833s, 803s, 754vs, 712m, 678m, 662m, 596m, 565s, 537s, 463vs; ^{1}H-NMR (ppm) in DMSO-d_6: 12.85 (s, H(N^1 and N^3) of MTUC), 7.54–6.92 (m, $H^{aromatic}$ and H(CH_3) of TOPT), 5.72 (s, H(C^3) of MTUC), 1.64 (w, H(CH_3-) of MTUC); UV-vis (DMSO): λ=296 nm (logε= 4.23) and λ=367 nm (logε= 3.55).

X-ray structure determination: Intensity data for the crystals of **1** were collected using an Oxford Diffraction CCD instrument, utilizing graphite-monochromated CuKa radiation (λ= 1.54184 Å). Cell parameters were determined via least-squares refinement of diffraction data extracted from 25 reflections. All data underwent correction for Lorentz-polarization effects and absorption (Oxford Diffraction Ltd, 2006). The structural elucidation involved utilizing direct methods with SHELXS97 (Sheldrick, 1990) and subsequent refinement through full-matrix least-squares procedures on F2 with SHELXL97 (Sheldrick, 1997).

Anisotropic refinement was applied to all non-hydrogen atoms, while hydrogen atoms were positioned at calculated sites and refined using the "riding model," with isotropic thermal parameters set at 1.2 (1.3 for CH_3 groups) times the Ueq value of the relevant carrier atom.

1: $C_{26}H_{26}ClN_2OPPdS$, MW= 587.37 g/mol, monoclinic, space group P21/n, a= 10.3919(3) Å, b= 22.4640(7) Å, c= 11.5973(3) Å, β= 94.880(2), V= 2,697.50(13) $Å^3$, Z= 4, T= 100 K, Radiation CuKα, ρ(calc)= 1.446 g cm^{-3}, μ= 7.903 mm^{-1}, F(000)= 1,192. 10776 reflections measured, 5132 unique (Rint= 0.082), 4,219 with I > 2s(I). The final R1= 0.0539 (for 4,219 reflections with I> 2s(I)) and wR2(F2)= 0.1887 (all data), S= 1.19.

Crystallographic data (excluding structure factors) for the structure reported in this paper has been deposited with the Cambridge Crystallographic Data Centre as supplementary publication no. CCDC-2303444 (**1**). Copies of the data can be obtained free of charge by application to CCDC, 12 Union Road, Cambridge CB2 1EZ, UK (fax: (+44) 1223-336-033; e-mail: deposit@ccdc.cam.ac.uk).

4.2 Biological tests

All biological tests were conducted following established protocols detailed in prior literature (Banti et al., 2015; Banti et al., 2016; Chrysouli et al., 2018; Stathopoulou et al., 2021; Kapetana et al., 2022; Banti et al., 2023; Banti et al., 2024). The preparation of solutions adhered to the procedures outlined in the respective references (Banti et al., 2015; Banti et al., 2016; Chrysouli et al., 2018; Stathopoulou et al., 2021; Kapetana et al., 2022; Banti et al., 2023; Banti et al., 2024). The SRB assay, cell morphology observations, and DNA binding studies using UV-vis and fluorescence spectroscopies were carried out according to previously established methodologies (Banti et al., 2015; Banti et al., 2016; Chrysouli et al., 2018; Stathopoulou et al., 2021; Kapetana et al., 2022; Banti et al., 2023; Banti et al., 2024). AO/EB Staining and the Permeabilization of the mitochondrial membrane test were performed following documented procedures (Stathopoulou et al., 2021; Kapetana et al., 2022; Banti et al., 2023; Banti et al., 2024). Viscosity and DNA Thermal Denaturation studies were conducted in line with previously published methods (Cory et al., 1985; Kelly et al., 1985; Banti et al., 2024).

Each biological experiment underwent at least three independent replications.

Data availability statement

The datasets presented in this study can be found in online repositories. The names of the repository/repositories and accession number(s) can be found in the article/Supplementary Material.

Ethics statement

Ethical approval was not required for the studies on humans in accordance with the local legislation and institutional requirements because only commercially available established cell lines were used.

Author contributions

CB: Investigation, Methodology, Supervision, Writing–original draft, Writing–review and editing. AT: Investigation, Writing–original draft. SH: Conceptualization, Data curation, Formal Analysis, Funding acquisition, Methodology, Project administration, Resources, Supervision, Validation, Visualization, Writing–original draft, Writing–review and editing.

Funding

The author(s) declare that no financial support was received for the research, authorship, and/or publication of this article.

Acknowledgments

The International PhD program, entitled "Biological Inorganic Chemistry (BIC)", is acknowledged. This program is co-financed by Greece and the European Union (European Social Fund- ESF) through the Operational Program «Human Resources Development, Education and Lifelong Learning 2014–2020» in the context of the subproject 6 "Biological Inorganic Chemistry (BIC)" (MIS 5162213).

Conflict of interest

The authors declare that the research was conducted in the absence of any commercial or financial relationships that could be construed as a potential conflict of interest.

The author(s) declared that they were an editorial board member of Frontiers, at the time of submission. This had no impact on the peer review process and the final decision.

Publisher's note

Supplementary material

The Supplementary Material for this article can be found online at: https://www.frontiersin.org/articles/10.3389/fchbi.2024.1338630/full#supplementary-material

References

Afsar, T., Trembley, J., Salomon, C., Razak, S., Khan, M. R., and Ahmed, K. (2016). Growth inhibition and apoptosis in cancer cells induced by polyphenolic compounds of Acacia hydaspica: involvement of multiple signal transduction pathways. *Sci. Rep.* 6, 23077. doi:10.1038/srep23077

Alam, M. N., and Huq, F. (2016). Comprehensive review on tumour active palladium compounds and structure–activity relationships. *Coord. Chem. Rev.* 316, 36–67. doi:10.1016/j.ccr.2016.02.001

Aulakh, J. K., Lobana, T. S., Sood, H., Arora, D. S., Kaur, R., Singh, J., et al. (2019). Silver derivatives of multi-donor heterocyclic thioamides as antimicrobial/anticancer agents: unusual bio-activity against methicillin resistant *S. aureus*, S. epidermidis, and *E. faecalis* and human bone cancer MG63 cell line. *RSC Adv.* 9, 15470–15487. doi:10.1039/c9ra01804b

Banti, C. N., Charalampou, D. C., Kourkoumelis, N., Owczarzak, A. M., Kubicki, M., Hadjikakou, S. K., et al. (2015). Mono-nuclear cis-Pd(II) chloride complex of the thio-nucleotide analogue 5-methyl-thiouracil and its biological activity. *Polyhedron* 87, 251–258. doi:10.1016/j.poly.2014.11.027

Banti, C. N., Papatriantafyllopoulou, C., Manoli, M., Tasiopoulos, A. J., and Hadjikakou, S. K. (2016). Nimesulide silver metallodrugs, containing the mitochondriotropic, triaryl derivatives of pnictogen; Anticancer activity against human breast cancer cells. *Inorg. Chem.* 55, 8681–8696. doi:10.1021/acs.inorgchem.6b01241

Banti, C. N., Papatriantafyllopoulou, C., Papachristodoulou, C., Hatzidimitriou, A. G., and Hadjikakou, S. K. (2023). New apoptosis inducers containing anti-inflammatory drugs and pnictogen derivatives: a new strategy in the development of mitochondrial targeting chemotherapeutics. *J. Med. Chem.* 66, 4131–4149. doi:10.1021/acs.jmedchem.2c02126

Banti, C. N., Piperoudi, A. A., Raptopoulou, C. P., Psycharis, V., Athanassopoulos, C. M., and Hadjikakou, S. K. (2024). Mitochondriotropic agents conjugated with NSAIDs through metal ions against breast cancer cells. *J. Inorg. Biochem.* 250, 112420. doi:10.1016/j.jinorgbio.2023.112420

Bera, B., Mondal, S., Gharami, S., Naskar, R., Das Saha, K., and Mondal, T. K. (2022). Palladium(II) and platinum(II) complexes with ONN donor pincer ligand: synthesis, characterization and *in vitro* cytotoxicity study. *New J. Chem.* 46, 11277–11285. doi:10.1039/d2nj01894b

Blanco, M. J. (2023). "New therapeutic modalities: transforming drug discovery and development," in *Drug discovery and evaluation: safety and pharmacokinetic assays*. Editors F. J. Hock, M. R. Gralinski, and M. K. Pugsley (Cham: Springer).

Blanco, M. J., and Gardinier, K. M. (2020). New chemical modalities and strategic thinking in early drug discovery. *ACS Med. Chem. Lett.* 11 (3), 228–231. doi:10.1021/acsmedchemlett.9b00582

Bomfim, L. M., de Araujo, F. A., Dias, R. B., Sales, C. B. S., Rocha, C. A. G., Correa, R. S., et al. (2019). Ruthenium(II) complexes with 6-methyl-2-thiouracil selectively reduce cell proliferation, cause DNA double-strand break and trigger caspase-mediated apoptosis through JNK/p38 pathways in human acute promyelocytic leukemia cells. *Sci. Rep.* 9, 11483. doi:10.1038/s41598-019-47914-x

Carneiro, T. J., Martins, A. S., Marques, M. P. M., and Gil, A. M. (2020). Metabolic Aspects of palladium(II) potential anti-cancer drugs. *Front. Oncol.* 10, 590970. doi:10.3389/fonc.2020.590970

Charalampou, D. C., Kourkoumelis, N., Karanestora, S., Hadjiarapoglou, L. P., Dokorou, V., Skoulika, S., et al. (2014). Mono- and binuclear copper(I) complexes of thionucleotide analogues and their catalytic activity on the synthesis of dihydrofurans. *Inorg. Chem.* 53, 8322–8333. doi:10.1021/ic500727z

Chen, Y., Li, L., Liu, Z., Liu, M., and Wang, Q. (2023). A series of ligustrazine platinum(IV) complexes with potent anti-proliferative and anti-metastatic properties that exert chemotherapeutic and immunotherapeutic effects. *Dalton Trans.* 52, 13097–13109. doi:10.1039/d3dt02358c

Chrysouli, M. P., Banti, C. N., Kourkoumelis, N., Panayiotou, N., Markopoulos, G., Tasiopoulos, A., et al. (2018). Chloro(triphenylphosphine)gold(I) a forefront reagent in gold chemistry as apoptotic agent for cancer cells. *J. Inorg. Biochem.* 179, 107–120. doi:10.1016/j.jinorgbio.2017.11.004

Correa, R. S., Bomfim, L. M., Oliveira, K. M., Moreira, D. R. M., Soares, M. B. P., Ellena, J., et al. (2019). Ru(II) complexes containing uracil nucleobase analogs with cytotoxicity against tumor cells. *J. Inorg. Biochem.* 198, 110751. doi:10.1016/j.jinorgbio.2019.110751

Cory, M., McKee, D. D., Kagan, J., Henry, D. W., and Miller, J. A. (1985). Design, synthesis, and DNA binding properties of bifunctional Intercalators. Comparison of Polymethylene and diphenyl ether chains connecting Phenanthridine. *J. Am. Chem. Soc.* 107, 2528–2536. doi:10.1021/ja00294a054

Dorairaj, D. P., Haribabu, J., Chang, Y.-L., Echeverria, C., Hsu, S. C. N., and Karvembu, R. (2022). Pd(II)–PPh_3 complexes of halogen substituted acylthiourea ligands: biomolecular interactions and *in vitro* anti-proliferative activity. *Appl. Organomet. Chem.* 36, e6765. doi:10.1002/aoc.6765

Espino, J., Fernández-Delgado, E., Estirado, S., de la Cruz-Martinez, F., Villa-Carballar, S., Viñuelas-Zahínos, E., et al. (2020). Synthesis and structure of a new thiazoline-based palladium(II) complex that promotes cytotoxicity and apoptosis of human promyelocytic leukemia HL-60 cells. *Sci. Rep.* 10, 16745. doi:10.1038/s41598-020-73488-0

Fanelli, M., Formica, M., Fusi, V., Giorgi, L., Micheloni, M., and Paoli, P. (2016). New trends in platinum and palladium complexes as antineoplastic agents. *Coord. Chem. Rev.* 310, 41–79. doi:10.1016/j.ccr.2015.11.004

Garoufis, A., Hadjikakou, S. K., and Hadjiliadis, N. (2009). Palladium coordination compounds as anti-viral, anti-fungal, anti-microbial and anti-tumor agents. *Coord. Chem. Rev.* 253, 1384–1397. doi:10.1016/j.ccr.2008.09.011

Groom, C. R., Bruno, I. J., Lightfoot, M. P., and Ward, S. C. (2016). The Cambridge structural database. *Acta Crystallogr. Sect. B Struct. Sci. Cryst. Eng. Mater.* 72, 171–179. doi:10.1107/s2052520616003954

Grosmaire, L., and Delarbre, J.-L. (2012). Vibrational spectra of 6-methyluracil, 6-methyl-2-thiouracil and their deuterated analogues. *J. Mol. Struct.* 1011, 42–49. doi:10.1016/j.molstruc.2011.12.007

Haribabu, J., Balakrishnan, N., Swaminathan, S., Dorairaj, D. P., Azam, M., Subarkhan, M. K. M., et al. (2023). Michael addition-driven synthesis of cytotoxic palladium(II) complexes from chromone thiosemicarbazones: investigation of anticancer activity through *in vitro* and *in vivo* studies. *New J. Chem.* 47, 15748–15759. doi:10.1039/d3nj02067c

Hernández, W., Vaisberg, A. J., Tobar, M., Álvarez, M., Manzur, J., Echevarría, Y., et al. (2016). *In vitro* antiproliferative activity of palladium(ii) thiosemicarbazone complexes and the corresponding functionalized chitosan coated magnetite nanoparticles. *New J. Chem.* 40, 1853–1860. doi:10.1039/c5nj02429c

Kapdi, A. R., and Fairlamb, I. J. S. (2014). Anti-cancer palladium complexes: a focus on PdX2L2, palladacycles and related complexes. *Chem. Soc. Rev.* 43, 4751–4777. doi:10.1039/c4cs00063c

Kapetana, M., Banti, C. N., Papachristodoulou, C., Psycharis, V., Raptopoulou, C., and Hadjikakou, S. K. (2022). Conjugation of triphenylantimony(V) with carvacrol against human breast cancer cells. *J. Biol. Inorg. Chem.* 27, 373–389. doi:10.1007/s00775-022-01936-5

Kasibhatla, S., Amarante-Mendes, G. P., Finucane, D., Brunner, T., Bossy-Wetzel, E., and Green, D. R. (2006). Acridine orange/ethidium bromide (AO/EB) staining to detect apoptosis. *Cold Spring Harb. Protoc.* 2006, pdb.prot4493. doi:10.1101/pdb.prot4493

Kelly, J. M., Tossi, A. B., McConnell, D. J., and OhUigin, C. (1985). A study of the interactions of some polypyridylruthenium(II) complexes with DNA using fluorescence spectroscopy, topoisomerisation and thermal denaturation. *Nucleic Acids Res.* 13, 6017–6034. doi:10.1093/nar/13.17.6017

Largy, E., Hamon, F., Rosu, F., Gabelica, V., De Pauw, E., Guedin, A., et al. (2011). Tridentate N-donor palladium(II) complexes as efficient coordinating quadruplex DNA binders. *Chem. – A Eur. J.* 17, 13274–13283. doi:10.1002/chem.201102300

Lazarevic, T., Rilak, A., and Bugarcic, Z. D. (2017). Platinum, palladium, gold and ruthenium complexes as anticancer agents: current clinical uses, cytotoxicity studies and future perspectives. *Eur. J. Med. Chem.* 142, 8–31. doi:10.1016/j.ejmech.2017.04.007

Moro, A. C., Watanabe, F. W., Ananias, S. R., Mauro, A. E., Netto, A. V. G., Lima, A. P. R., et al. (2006). Supramolecular assemblies of cis-palladium complexes dominated by CH···Cl interactions. *Inorg. Chem. Commun.* 9, 493–496. doi:10.1016/j.inoche.2006.02.012

Oxford Diffraction Ltd (2006). *(release 28-08- 2006 CrysAlis171.NET), Oxford diffraction, crysalis CCD and crysalis RED*. Abingdon, Oxford, England: Oxford Diffraction Ltd. Version p171.29.2.

Papazoglou, I., Cox, P. J., Hatzidimitriou, A. G., Kokotidou, C., Choli-Papadopoulou, T., and Aslanidis, P. (2014). Copper(I) halide complexes of 5-carbethoxy-2-thiouracil: synthesis, structure and *in vitro* cytotoxicity. *Eur. J. Med. Chem.* 78, 383–391. doi:10.1016/j.ejmech.2014.03.052

Pruchnik, H., Lis, T., Latocha, M., Zielińska, A., and Pruchnik, F. P. (2016). Palladium(II) complexes with tris(2-carboxyethyl)phosphine, structure, reactions and cytostatic activity. *J. Inorg. Biochem.* 156, 14–21. doi:10.1016/j.jinorgbio.2015.12.001

Schlagintweit, J. F., Jakob, C. H. G., Meighen-Berger, K., Gronauer, T. F., Weigert Muñoz, A., Weiß, V., et al. (2021). Fluorescent palladium(ii) and platinum(ii) NHC/1,2,3-triazole complexes: antiproliferative activity and selectivity against cancer cells. *Dalton Trans.* 50, 2158–2166. doi:10.1039/d0dt04114a

Shaheen, F., Badashah, A., Gielen, M., Marchio, L., de Vos, D., and Kaleem Khosa, M. (2007). Synthesis, characterization and *in vitro* cytotoxicity of homobimetallic complexes of palladium(II) with 2-thiouracil ligands. Crystal structure of [Pd2(TU)(PPh3)3Cl2]. *Appl. Organomet. Chem.* 21, 626–632. doi:10.1002/aoc.1227

Sheldrick, G. M. (1990). Phase annealing in SHELX-90: direct methods for larger structures. *Acta Crystallogr. Sect. A Found. Crystallogr.* 46, 467–473. doi:10.1107/s0108767390000277

Sheldrick, G. M. (1997). *SHELXL-97, program for the refinement of crystal structures*. Göttingen, Germany: University of Göttingen.

Sheng, X., Lu, X., Chen, Y., Lu, G., Zhang, J., Shao, Y., et al. (2007). Synthesis, DNA Binding, Cleavage, and Cytotoxic Activity of New 1,7-Dioxa4,10-diazacyclododecane artificial receptors containing bisguanidinoethyl or diaminoethyl double side arms. *Chem. – A Eur. J.* 13, 9703–9712. doi:10.1002/chem.200700549

Stathopoulou, M. E. K., Zoupanou, N., Banti, C. N., Douvalis, A. P., Papachristodoulou, C., Marousis, K. D., et al. (2021). Organotin derivatives of cholic acid induce apoptosis into breast cancer cells and interfere with mitochondrion; Synthesis, characterization and biological evaluation. *Steroids* 167, 108798. doi:10.1016/j.steroids.2021.108798

Wang, Z., Li, J., Liu, R., Jia, X., Liu, H., Xie, T., et al. (2023). Synthesis, characterization and anticancer properties: a series of highly selective palladium(II) substituted-terpyridine complexes. *J. Inorg. Biochem.* 244, 112219. doi:10.1016/j.jinorgbio.2023.112219

Zhu, Z., Wang, Z., Zhang, C., Wang, Y., Zhang, H., Gan, Z., et al. (2019). Mitochondrion-targeted platinum complexes suppressing lung cancer through multiple pathways involving energy metabolism. *Chem. Sci.* 10, 3089–3095. doi:10.1039/c8sc04871a

Zielonka, J., Joseph, J., Sikora, A., Hardy, M., Ouari, O., Vasquez-Vivar, J., et al. (2017). Mitochondria-targeted triphenylphosphonium-based compounds: syntheses, mechanisms of action, and therapeutic and diagnostic applications. *Chem. Rev.* 117, 10043–10120. doi:10.1021/acs.chemrev.7b00042